Beam-size effects on the measurement of sub-picosecond intrinsic laser induced damage threshold of dielectric oxide coatings

Marek Stehlík, Frank Wagner, Janis Zideluns, Fabien Lemarchand, Julien Lumeau, Laurent Gallais

Investigation of beam-size effects on the measurement of sub-picosecond intrinsic laser induced damage threshold of dielectric oxide coatings

MAREK STEHLÍK[1], FRANK WAGNER[1], JANIS ZIDELUNS[1], FABIEN LEMARCHAND[1], JULIEN LUMEAU[1], AND LAURENT GALLAIS[1,*]

[1] Aix Marseille Univ, CNRS, Centrale Marseille, Institut Fresnel, Marseille, France
[*] Corresponding author: gallais@fresnel.fr

Compiled August 24, 2021

Laser-induced damage experiments on HfO_2 and Nb_2O_5 thin films were performed with 500 fs pulse duration at 1030 nm wavelength. Threshold fluences as a function of beam size have been determined for effective beam diameters ranging from 40 to 220 μm, in single shot regime. The results suggest no beam size effect related to material properties in the investigated range, but size effects related to the metrology. The results indicate the importance of appropriate focusing conditions and beam measurement to qualify the optics for use in lasers with large beam sizes.

http://dx.doi.org/10.1364/ao.XX.XXXXXX

1. INTRODUCTION

Since the early years of laser research, laser damage has been a phenomenon that has been extensively studied. [1] The studies focusing on determination of laser-induced damage threshold (LIDT) are important for proper handling of optical components in laser systems [2] and for the research on material processing [3] comprising ablation and laser machining. [4] It was soon recognized that laser-induced damage in optical components is usually initiated by defects, such as pits, grooves, cracks, absorbing inclusions, scratches, pores, impurities or material contamination. [5–10] The defects, that act as laser damage precursors, are inherently stochastically distributed and thus provide explanation of non-deterministic behavior and damage threshold dependence on laser beam size. [6, 11] Larger beams increase the probability that a defect is present within the irradiated area. The defect dominated damage behavior was observed in long-pulse (nanosecond) regime, in which the damage is consequence of several physical processes involving absorption, heating, phase changes of materials, hydrodynamic processes and plasma formation. Since nanosecond pulses are relatively long compared to the time scales of these processes, small defect precursors can trigger a cascade of events that can lead to micro-explosion and damage. [12, 13] However, if the pulse duration is shorter than the relaxation time, i.e. energy transfer from electrons to atomic network, which lasts several picoseconds for dielectrics, the processes of excitation and relaxation are decoupled in time. [14] In such ultra-short regime, the damage is mainly driven by multiphotonic absorption in the irradiated material because the other processes cannot be involved within the short pulse duration. Laser damage with sub-ps pulses has therefore a strong nonlinear dependence on intensity and the damage threshold fluence is deterministic without significant statistical variations, as opposed to nanosecond pulses. [15–19] The evidence of deterministic damage threshold suggests that damage initiation is given by fundamental intrinsic material properties (energy bandgap, refractive index) rather than by stochastically distributed defects. Thus, if the limiting factor of material damage resistance seems to be the intrinsic material properties, then the laser damage threshold is expected to be independent on laser beam size. This was confirmed in the early studies on this topic with fused silica irradiated by 400 fs pulses within the beam diameters ranging from 0.4 to 1.0 mm. [20] The fused silica LIDT independence on beam size was confirmed at 100 fs with number of pulses ranging from 1 to 1000. [21]

However, this attitude to damage onset initiated by ultrashort pulses might not be entirely correct. There are experimental studies employing pulses of duration between 30 fs and 1 ps showing damage/ablation thresholds dependent on the beam size. These experiments were done on stainless steel [28, 29], silicon [28, 29], or even dielectric materials (fused silica [22], barium borosilicate glass [25], ion phosphate glass [26], dentin [30], sapphire monocrystal [23], polystyrene [31]). In the studies [22, 25, 26, 28, 29, 31] the beam size dependence of laser damage was described using defect-site models distinguishing two laser-induced damage regimes - extrinsic defect-dominated regime for larger beam sizes and intrinsic regime for smaller ones. The defect-site models fitted well the experimental results, even though the nature of defect sites initiating damage remains

Table 1. Review of some studies on beam size effect on damage threshold by ultrashort pulses. Symbols: τ - pulse duration, λ - laser wavelength, Non1 - number of pulses irradiated on the same site, f - pulse repetition rate. For more details, see references.

Material - reference	LIDT	Beam diameter	Beam size	τ	λ	Non1	f	Explanation
[-]	[J/cm^2]	[μm]	effect [-]	[fs]	[nm]	[-]	[kHz]	[-]
Fused silica [22]	26 – 6	1.6 – 22	Yes	450	1025	1	-	Defects
Sapphire crystal [23]	45 – 1	6 – 110	Yes	100	800	1	1	Plasma shielding
Fused silica [24]	6.5 – 6	30 – 100	$< 15\,\%$	1000	1053	1	-	
E-beam Si coating [24]	5.5 – 5	30 – 100	Ambiguous	1000	1053	1	-	
PIAD Si coating [24]	4.5 – 4	30 – 100	Ambiguous	1000	1053	1	-	
Borosilicate glass [25]	1.0 – 0.2	40 – 800	Yes	30	800	1000	1	Defects
Ion phosphate glass [26]	0.8 – 0.3	160 – 560	Yes	30	795	1000	1	Defects
Fused silica [20]	2.3	400 – 1000	No	400	1053	600	0.01	
Fused silica [21, 27]	$\sim$ shots	5.6; 23	No	100	800	1-1k	≤ 0.02	

often unclear. [25, 26, 32] In the work [29], the effect of material treatment on the damage threshold was studied. Both the AlO_x slurry treatment on silicon and grit sandpaper treatment on stainless steel led to an increase of defect density, increasing the effect of beam-size on LIDT. The effects of defects in the studies (Table 1) are the potential explanations, but they are not demonstrated. The role of defects in dentin [30], stainless steel [28, 29], polystyrene [31] or slurry treated silicon [29] could be affected by the fact that the opaque materials do not show optical quality or sample homogeneity. In addition, the multiple shot tests reflect presence of cumulative effects including laser-induced defects that facilitate process of electronic excitation which differs from fundamental interaction of a sub-ps pulse with a monolayer of dielectric material that we aim to study in this work. In the study of damage threshold on dentin [30], the effect of beam size was significantly affected by repetition rate. At 100 Hz, the ablation threshold was almost independent on beam size whereas at higher repetition rates, 1 kHz and 500 kHz, the beam size dependence of ablation thresholds was evident and heat accumulation was proposed as an explanation. Recently, E-beam deposited and PIAD silica thin films together with fused silica were tested by broad range of picosecond pulse durations (1 – 60 ps) and results were compared for three sizes of beam waists (30, 50, 100 μm in FWHM). [24] The results obtained by 1 ps pulses are ambiguous with respect to the beam size effect. The highest threshold fluences were measured with smallest beams (30 μm) in all three optical materials but the thresholds achieved with 50 μm beam waists were lower than the 100 μm ones for both coatings.

The comparison of above mentioned published results (Table 1) is difficult since the experiments have not been done in the same conditions. The laser parameters differed in pulse duration, laser wavelength, number of pulses, repetition rate or spot size range. The tests were done on various samples of different properties (material, surface state, fabrication, polishing, cleaning, contamination, prior history etc.). The study of beam-size dependence in femtosecond range could be also affected by nonlinear effects which were observed in bulk fused silica below damage threshold in the case of smaller numerical apertures, i.e. larger beam sizes. [33] Apart from the experimental conditions, the laser damage dependence on beam size is a function of the used threshold definition. The results published in nanosecond study [34] suggest damage threshold independence of beam size if damage threshold is defined as fluence of 0 % damage probability. However, if damage threshold is considered as fluence of 50 % damage probability, the effect of beam-size is evident. In general, the effect of beam size is growing with increasing probability of damage used for threshold definition. Additionally, the damage threshold results may vary by a few percents because of used calorimeters or beam profiling cameras that have influence on possible deviations of measured pulse energies or beam areas. [35]

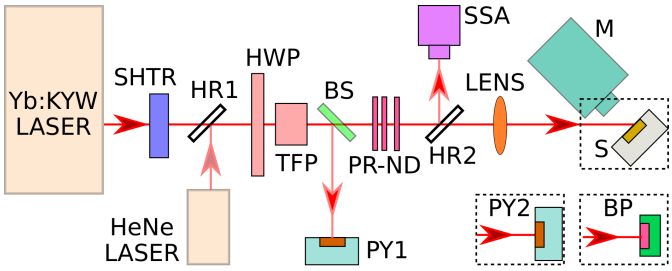

Fig. 1. Schematic drawing of sub-ps near-infrared LIDT station. HeNe laser is intended for station alignment. SHTR - shutter, HR1/HR2 - high reflective flip-flop mirrors, HWP - half-wave plate, TFP - thin film polarizer, BS - beam splitter, PY1/PY2 - pyroelectric detectors, PR-ND - partially reflective @1030nm and neutral density filters, LENS - focusing lens, S - sample, BP - beam profiling camera, SSA - single shot autocorrelator. More details are given in Section A.

The motivation of this study is to test laser damage resistance of dielectric materials that are used in coatings of optical components which determine the limit of reliable operation of high energy sub-picosecond solid-state lasers. [2] The effect of beam size on the damage threshold is extremely important for qualifying optical components for mass use in high power lasers. The results in this work should indicate whether small beam sizes can be used for the testing of optical components that will be implemented in high-energy large-beam lasers. The limit to this approach is the role of macroscopic defects, such as nodules, that were evidenced in the sub-ps regime. [36] In that case only Raster scan testing procedures are relevant for laser damage testing. [37] We will focus on the single shot testing method to study fundamental interaction of a sub-picosecond pulse with a monolayer of dielectric material (HfO_2, Nb_2O_5) and to exclude the complexity of cumulative effects and interference phenomenon in a multilayer stack.

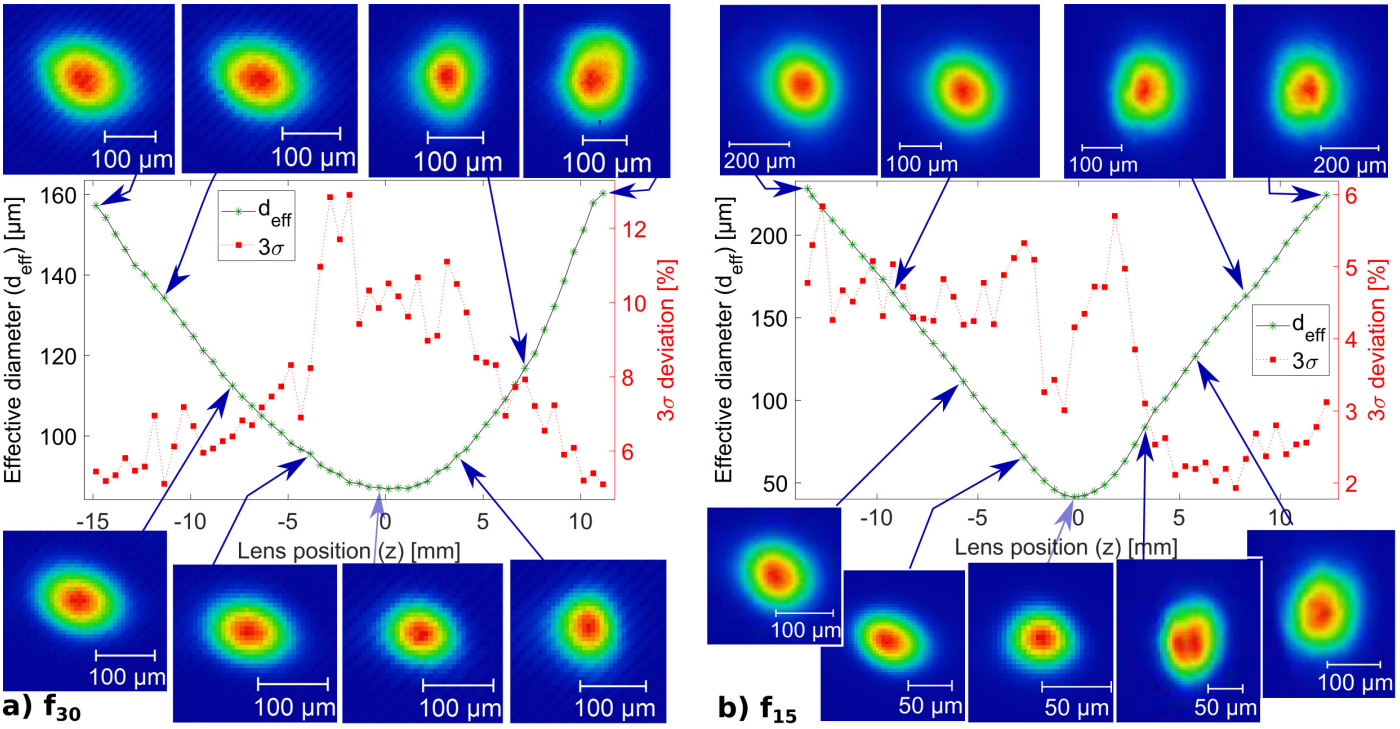

Fig. 2. Effective beam diameter (d_{eff}) and 3x standard deviation (3σ) of effective area as a function of lens position, with typical normalized beam profiles at different positions. For $z < 0$, the camera is close to the focusing lens (before the focal plane). Comparison of lenses with different focal lengths: a) $f_{30} = 30\,\text{cm}$, $d_{\text{eff,min}} \approx 40\,\mu\text{m}$, b) $f_{15} = 15\,\text{cm}$, $d_{\text{eff,min}} \approx 86\,\mu\text{m}$.

2. DESCRIPTION OF EXPERIMENT AND METHODS

A. Experimental set-up

Laser damage tests were done by using a commercial diode pumped Yb:KYW laser (Amplitude Systemes S-pulse HP). The system emits radiation of nearly Gaussian spatial profile in the near-infrared wavelength around 1030 nm. The emitted pulses have pulse duration of 500 ± 50 fs that was measured by a single shot autocorrelator (AVESTA ASF 70 fs–3 ps, Acore software). The experimental set-up is described in Fig. 1.

We used the Yb:KYW laser at 10 Hz repetition rate. The maximum pulse energy was 1 mJ. The single shot mode was achieved using a mechanical shutter (SHTR, Thorlabs SH05). The pulse energy was adjusted by a 0-order half-wave plate (HWP), mounted on a motorized rotation stage, and a thin-film polarizer (TFP). The beam that passed through the polarizer falls on the beamsplitter (BS) which directs a small part of pulse energy (5 %) to a pyroelectric energy meter (OPHIR PE9) recording the energy of each pulse. The energy meter is calibrated to the energy incident on the tested sample (S) which was measured using a second pyroelectric meter (PY2, OPHIR PE9F) placed behind a focusing lens (LENS).

The beam used for LIDT testing is linearly polarized and focused by a plano-convex lens on the tested sample (S) which was placed at 45° incidence angle. The LIDT testing was performed in ambient air at room temperature. Positioning of the tested sample near focal plane is done using a motorized 2D translation stage. The laser damage station is equipped with a He-Ne laser which is used for beam alignment.

The focused laser radiation of pulse energy reduced by 6 to 7 orders of magnitude using a combination of partially reflective at 1030nm and neutral density filters (PR-ND) is analyzed by a beam profiling camera (BP) connected to an imaging software. The camera was placed instead of holder with sample (S), see Fig. 1, and its sensor was oriented perpendicularly to the beam direction. In this study, two focusing plano-convex lenses with focal lengths of 30 cm and 15 cm were used separately. Both lenses had 25 mm diameter and were AR coated. Examples of measured beam profiles at different lens positions for both lenses are shown on Fig. 2. For $z < 0$, the camera is close to the focusing lens (before the focal plane).

B. Tested samples

The tested samples were monoloayers of HfO_2 and Nb_2O_5. The HfO_2 sample of 150 nm thickness was deposited by electron-beam evaporation with ion assistance on BK7 substrate. Refractive index is 1.93 determined at 1053 nm with spectrophotometry. [38] The Nb_2O_5 monolayer was deposited on fused silica substrate with magnetron sputtering process controlled by HELIOS system. [39] The refractive index was determined by spectrophotometry to be 2.26 at 1030 nm wavelength. The thickness of tested Nb_2O_5 layers was 150 and 450 nm.

C. Beam size measurement

Particular attention in this study was given to the determination of beam size with its statistical deviation in dependence of lens position. The beam size is expressed using the effective diameter (d_{eff}), defined using square root of the effective area (A_{eff}) divided by π: [40]

$$d_{\text{eff}} = 2 \cdot \sqrt{\frac{A_{\text{eff}}}{\pi}}. \tag{1}$$

For beam with transverse profile of optical intensity described using Gaussian function, the diameter at $1/e^2$ peak intensity is $d_{1/e^2} = \sqrt{2} \cdot d_{\text{eff}}$. The effective area is obtained by the ratio of

Table 2. Parameters of beam profilers.

Camera	WinCam	BP87
Sensor type	CCD 14-bit	CMOS 12-bit
Pixel size [μm]	6.45 x 6.45	3.45 x 3.45
Exposure time	41 μs	39 μs
Noise per signal max.	1-2%	0.1%

pulse energy E and maximum energy density ($F_{\max}$) of the laser pulse in the target plane, i.e. [40]

$$A_{\text{eff}} = \frac{E}{F_{\max}} = \frac{\sum_{\text{pixel}} E_{\text{pixel}}}{\frac{E_{\max}}{S_{\text{pixel}}}}, \tag{2}$$

where E_{pixel} is the signal measured on a pixel, S_{pixel} denotes the surface of one pixel and $E_{\max}$ stands for maximum signal of the beam captured on one pixel of used sensor.

For both used lenses, the beam profiles were measured at discrete lens positions with maximum lens position step of 0.5 mm. The beam profile after lens of 30 cm focal length, see Fig. 2a), was measured by WinCam UCD23 camera (DataRay Inc.) with CCD sensor of 6.45 μm pixel length. In the case of lens with 15 cm focal length, the beam profiles were analyzed by two different cameras: the WinCam UCD23 and BP87 (Femto Easy) whose parameters are listed in Table 2. The results recorded by these cameras were analogous but the ones of BP87 were preferred because the used CMOS sensor provided higher lateral resolution due to its 3.45 μm pixel length, which was important for the smallest beam around the focal plane. Another advantage of BP87 beam profiler was its lower noise in comparison to the WinCam. The statistical results, see Fig. 2b), were derived from 100 frames per one lens position.

The measurement of effective area in dependence of lens position allowed us to determine accurately focal plane corresponding to the lens position with minimum of effective area. The obtained data points of effective beam area were then linearly interpolated between each measured point in order to determine subsequently the effective beam areas of specific lens positions corresponding to the LIDT tests.

The values of three standard deviations (3σ) from a mean were calculated using the formula:

$$3\sigma = 3 \cdot \sqrt{\frac{\sum_{i=1}^{N} (A_i - \bar{A})^2}{N-1}}, \tag{3}$$

where A_i represents i-th area value and $\bar{A}$ the average (mean) area value within the sample size of N values, i.e. number of beam profile frames per given lens position. The 3σ deviations were also linearly interpolated between each measured point to be defined at lens positions corresponding to the LIDT tests. Thus, the 3σ deviations shown in LIDT results are only estimations since they were not measured at exactly the same lens positions.

D. Laser stability

The accuracy of damage threshold depends on the laser stability. Instabilities in temporal or spatial beam profile can affect damage threshold and lead to erroneous results. [41] The stability parameters of used near-infrared LIDT station were measured and their 3σ deviations are summarized in Table 3. Thanks to the low variations in pulse energy, pulse duration and beam size, the station enables to perform laser damage tests with high accuracy and limits the errors in measurement.

Table 3. Variations of laser stability parameters, expressed in pulse-to-pulse 3σ deviations. Effective beam area was measured for two lenses of different focal length (f). The 3σ deviation of effective area depends on lens position, see Fig. 2. Sampling expressed in number of pulses.

Parameter	f	3σ	Sampling
Effective area	30 cm	$< 13\,\%$	64 / lens pos.
	15 cm	$< 6\,\%$	100 / lens pos.
Pulse energy		0.7 %	30000
Pulse duration		1.2 %	1600

E. Damage test procedure

The LIDT test consisted of a procedure adapted to the study of beam size effect on damage threshold. The different beam sizes were achieved by focal lens positioning on the motorized stage. At a given lens position, the sample was irradiated at different spots with unique pulse energies that were changed with $\sim 1\,\%$ energy increment. The damage threshold was then determined as an average between the lowest fluence with damaged spot and the highest fluence with zero probability of damage. The LIDT results on both Nb_2O_5 and HfO_2 were deterministic.

F. Damage detection

The laser damage was detected *in situ* by optical microscopy with a 20x magnification of objective mounted on BXFM Olympus microscope. The technique allows real time estimation of the irradiated sample surface state. After the LIDT testing, an *ex-situ* damage inspection was performed using an Zeiss Axiotech differential interference contrast microscope with objective of 20x magnification. The *ex-situ* observation technique was preferred for the determination of damage threshold results presented in this work.

G. Fluence evaluation

The F_{ext} external energy density (or fluence) at the laser induced damage threshold is obtained by dividing E pulse energy by A_{eff} effective area of beam, see Eq. (2), as defined in the international standards: [40]

$$F_{\text{ext}} = \frac{E}{A_{\text{eff}}}. \tag{4}$$

The relative uncertainty of the damage threshold fluence is thus obtained from the uncertainties of pulse energy and effective area as:

$$\frac{\Delta F_{\text{ext}}}{F_{\text{ext}}} = \frac{\Delta E}{E} + \frac{\Delta A_{\text{eff}}}{A_{\text{eff}}}. \tag{5}$$

In this work, we express the inaccuracies using 3σ values.

H. Intrinsic LIDT fluence

Since the optical layers are the scene of interferential effects, the distribution of electric field inside layer irradiated by laser is not homogeneous. The electric field distribution is critical for understanding the sub-ps LIDT results because the excitation of dielectrics is governed by electronic processes. [42] To compare LIDT results with different conditions having an influence on

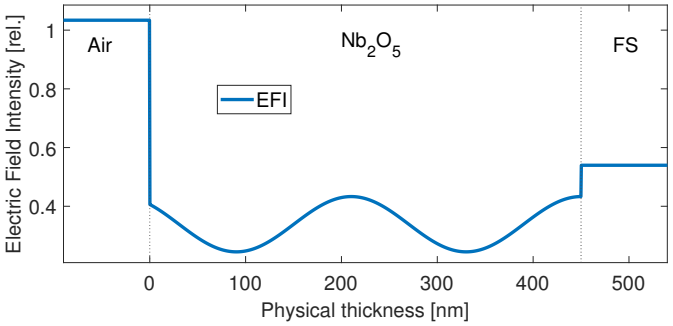

Fig. 3. Distribution of electric field intensity (EFI) inside Nb_2O_5 layer of 450 nm thickness (refractive index 2.26 at 1030 nm). Fused silica substrate (FS, refractive index 1.45 at 1030 nm). Polarization P, angle of incidence 45°. The EFI is normalized to the incident electric field amplitude in air.

electric field distribution, e.g. angle of incidence, polarization, layer thickness or refractive index, it is necessary to rescale the LIDT results with the electric field intensity maximum ($EFI_{\max}$) within the given layer. Therefore, the fluence values reported in this study correspond to F_{int} intrinsic fluence determined using F_{ext} external fluence and the $EFI_{\max}$:

$$F_{\text{int}} = EFI_{\max} \cdot F_{\text{ext}} = \left| \frac{E_{\max}}{E_{\text{inc}}} \right|^2 \cdot F_{\text{ext}}, \qquad (6)$$

where the $E_{\max}$ represents the maximum value of electric field in the layer and the E_{inc} means incident electric field amplitude. [43] The correction factor of incidence angle is taken into account within the $EFI_{\max}$ calculation. The distribution of electric field intensity for used Nb_2O_5 layer with our experimental conditions is shown on Fig. 3.

I. Match LIDT pulse energies to effective areas

Since the effective area was measured at discrete lens positions before or after the LIDT tests, it was needed to match the effective area data to the LIDT energies. To do that, we firstly determined the z lens position coordinate, for which the effective beam area was smallest ($z = 0$). Knowing the effective areas before ($z < 0$) and after ($z > 0$) the lens focal length, we described the evolution of effective areas in both directions from the waist. Then we tried to shift the data of LIDT pulse energies to correspond well to the evolution of effective beam areas as it is shown on Fig. 4. The results clearly show high sensitivity of determined fluences on the lens position shift and should be considered as a significant source of fluence inaccuracy in this work.

3. EXPERIMENTAL RESULTS AND DISCUSSION

A. Results with 30 cm focal length

The LIDT testing by lens with 30 cm focal length was repeated three times for HfO_2 sample. The results of tests 1 and 2 were evaluated using the preferred *ex-situ* DIC microscopy while the ones of test 3 correspond to the *in-situ* damage detection. The LIDT results on Fig. 5 underline the critical effect of damage detection on LIDT determination. In our case it adds an offset that seems consistent. Fig. 5a) illustrates the damage threshold pulse energies together with effective area values in dependence of lens position. Both effective area and damage threshold energies indicate similar dependence on increasing distance from focal plane. The behavior can be evidenced by independence

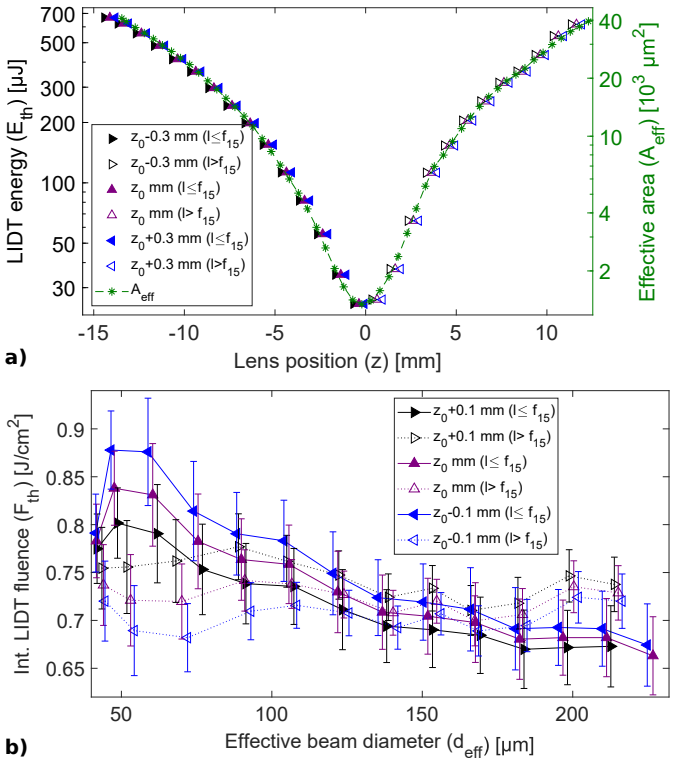

Fig. 4. LIDT results of Nb_2O_5 sample tested with lens of $f_{15} = 15$ cm focal length: a) Fitting of LIDT pulse energy dataset to the A_{eff} effective area curve using a linear relationship between them, b) Influence of shift in lens position by 0.1 mm to the intrinsic LIDT fluence with respect to effective beam radius. Symbols: z_0 means one specific lens position, l is distance from lens to the surface of tested sample.

of intrinsic LIDT fluence on the beam size as shown on Fig. 5b). The small deviations ($< 10\%$) for larger effective beam radii (> 65 µm) could be connected with beam divergence influencing angle of incidence and thus EFI maxima. Also the real beam size at the spot on tested sample can be different since the sample was inclined at 45° and beam position slightly shifts in dependence on lens position. However, the observed deviations of intrinsic LIDT fluences are still in compliance with the shown error bars summarizing 3σ deviation of effective beam area, 3σ deviation of pulse energy and uncertainty given by $\sim 1\%$ energy increment in damage test procedure. For this measurement, we thus do not see a significant beam size effect on intrinsic LIDT fluence.

B. Results with 15 cm focal length

The beam-size effect on LIDT fluence was studied also with lens of 15 cm focal length. The results for Nb_2O_5 and HfO_2 samples are shown on Figs. 6a) and 6b), respectively. In contrast to the previous results with the lens of 30 cm focal length (Fig. 5), the interpretation of LIDT fluences in dependence of beam size is difficult in the case of lens with 15 cm focal length since we observe differences of threshold values up to 20 % around focal plane. Also, for the large beam sizes, we see differences in LIDT values between tests performed with lens-sample distances smaller and larger than focal length. In the following sections we shall analyse the possible cause of LIDT deviation when changing the spot size.

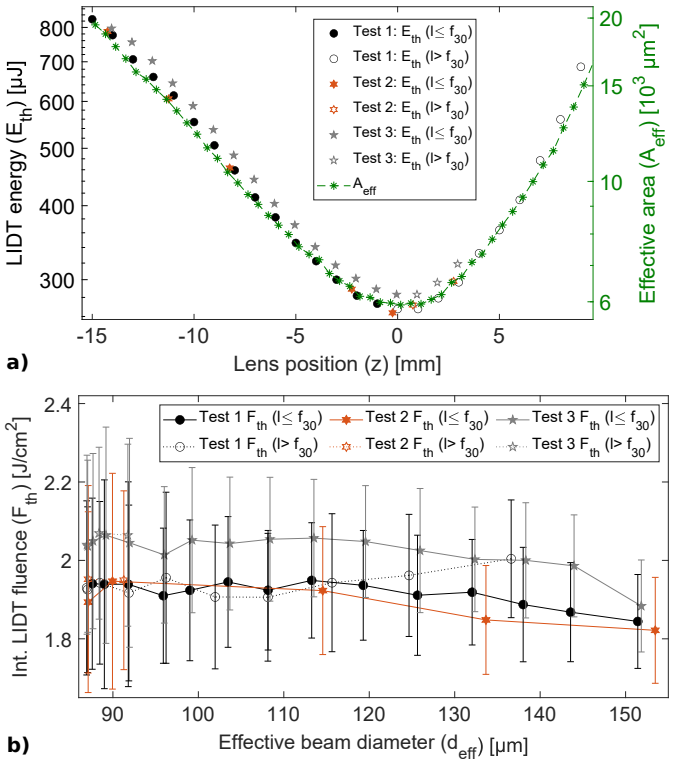

Fig. 5. Summary of LIDT results with HfO_2 sample tested by lens of $f_{30} = 30$ cm focal length: a) LIDT energy and effective area as a function of lens position. The two y axis are linked by linear scaling law. Figure b) shows the intrinsic LIDT fluence in dependence of effective beam radius. Tests 1 and 2 were evaluated using the preferred *ex-situ* microscopy. Test 3 corresponds to the *in-situ* damage detection. Length l means distance from lens to the tested sample surface.

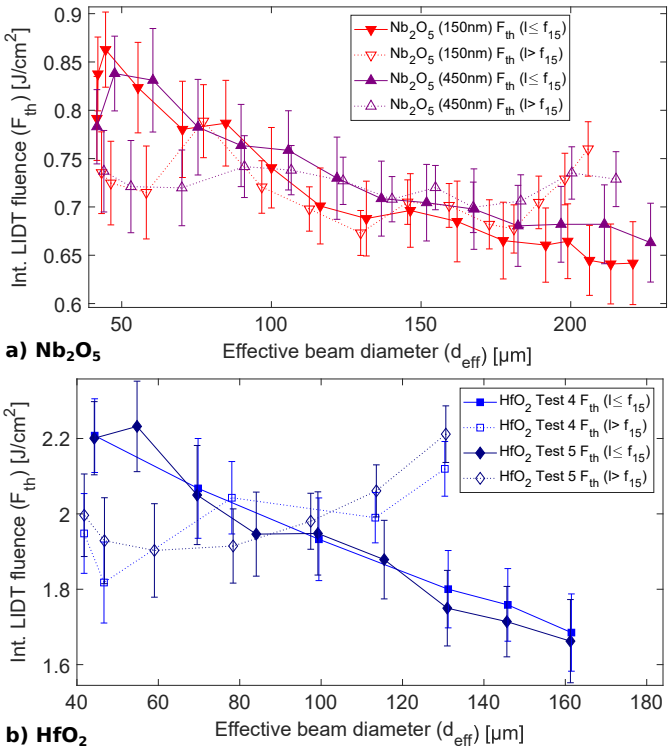

Fig. 6. Summary of intrinsic LIDT results obtained using the lens of $f_{15} = 15$ cm focal length: a) intrinsic LIDT of two Nb_2O_5 coatings of different thicknesses ($\bigtriangledown$ 150 nm, $\bigtriangleup$ 450 nm) obtained in two different LIDT test campaigns, b) intrinsic LIDT fluence of HfO_2 sample determined in two different LIDT test campaigns. The $\bigtriangleup$ and $\diamond$ datasets were obtained with very accurately aligned beam whose maximal shift of peak caused by lens positioning was around 30 μm. In the case of $\bigtriangledown$ and $\square$ tests, it was around 400 μm.

C. Analysis of potential self-focusing effects in air

Since the sub-picosecond systems have high peak powers of pulses, they can create conditions for nonlinear effects that can modify the beam profile. The important phenomenon, that can introduce errors in the damage testing, is self-focusing. The evaluation of self-focusing for Gaussian beams is possible by estimating self-focusing power: [44]

$$P_{SF} = \frac{0.149\lambda^2}{n_2 n_0}, \tag{7}$$

where n_0 signs for linear refractive index and n_2 is nonlinear refractive index of air, defined by $n = n_0 + n_2 I$, where I means intensity.

For femtosecond pulses (≤ 200 fs) at 800 nm wavelength, the nonlinear refractive index n_2 of air can be found in several publications [45–48], in which its value ranges between 10^{-23} and $6 \cdot 10^{-23}$ m^2/W in dependence on wavelength, pulse duration or refractive index measurement method. [49] In 2014, Mitrofanov et al.[50] determined the nonlinear refractive index of air to be $n_2 \sim 5 \cdot 10^{-23}$m^2/W at 1030 nm wavelength, 200 fs pulse durations, which are parameters close to the irradiation conditions of our LIDT setup (540 fs pulse duration, 1030 nm wavelength). Substituting the value in Eq. (7), the self-focusing power for our setup is $P_{SF} \sim 3.2$ GW, that is 2 times larger than the highest used peak power of 1.6 GW corresponding to pulse energy of 0.85 mJ. Thus, the beam propagation should not be exposed to self-focusing phenomenon in air. In addition, this question is relevant only in the case of LIDT testing at sample-lens distances larger than focal length with pulse energies close to our maximum, i.e. for the largest beam sizes.

D. Self-focusing effects in the lens

A potential cause of the evolution of LIDT with spot size could be self focusing in the lens material. If our results are affected by the effect, the influence is largest for the highest pulse energies that correspond to the farthest lens positions from the focus. For the sample-lens distances closer than focal length ($l < f_{15}$), the effect can cause more intense focusation and lower damage threshold energy. Since the beam profile measurement was performed with pulse energies reduced by 6-7 orders of magnitude compared to the LIDT tests, the determined effective areas may not correspond to the real ones affected by self-focusing. The effect could thus be interpreted as decrease of intrinsic LIDT fluence for the lowest sample-lens distances ($z < 0$) as it is shown on Fig. 7.

The more intense focusation can thus lead to shift of focal plane to shorter sample-lens distances but also to faster defocusation in dependence on z posititon. Therefore, the LIDT thresholds could be higher for the largest sample-lens distances ($z > 0$) which correlates with the results on Fig. 7.

For the effective beam diameters in the range from 75 μm to

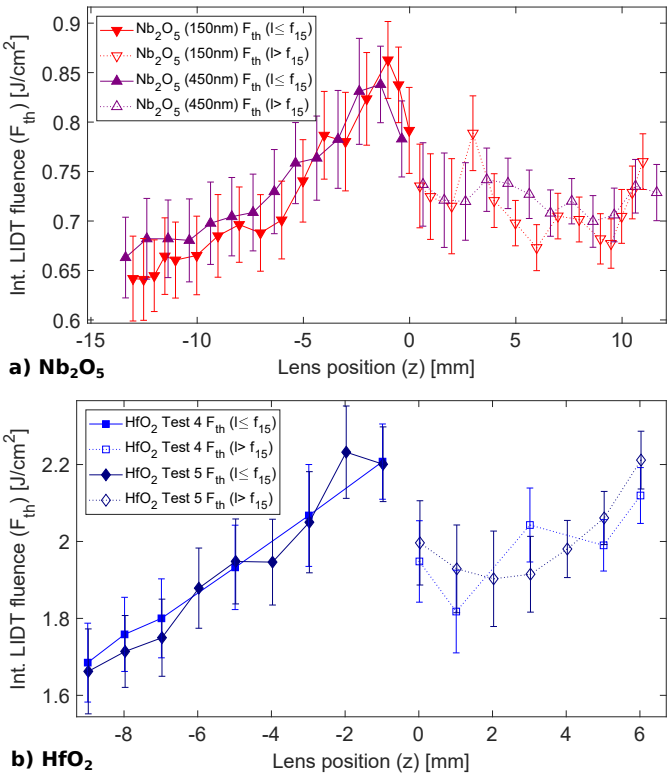

Fig. 7. Intrinsic LIDT fluence results for a) Nb_2O_5 and b) HfO_2. The results are the same as in Fig. 6, but here they are plotted as a function of z lens position.

175 µm, see Fig. 6, the more pronounced discrepancy between the damage thresholds before and after the focal length in the case of HfO_2 sample than in the Nb_2O_5 tests correlates with the higher pulse energies in the HfO_2 tests. This also suggest a potential self-focusing effect since the damage threshold energies of HfO_2 were approximately 3 times larger for the same beam diameter.

E. Effect of beam divergence

In the LIDT determination procedure, it is assumed that a plane wave propagates in the sample to calculate the electric field distribution. Because of the Gaussian nature of the laser beam, this is not the case when LIDT tests are performed out of the focal plane. We have therefore tried to estimate the consequences on EFI calculation.

Assuming that our beam is close to the Gaussian beam profile (see Fig. 2b), and characterized with a certain M^2 factor, we can calculate the θ divergence half-angle using the relation:

$$\theta = M^2 * \frac{\lambda}{\pi w_0}, \tag{8}$$

where w_0 stands for $1/e^2$ beam radius at the beam waist. The meaning of half-divergence angle is that the angle from beam axis should cover 86.5% of the pulse energy in the case of ideal gaussian beam in far field from focal plane. It could thus be assumed that the half-divergence angle would also define the range of incidence angles and positions where the material damage is initiated. For our beam, the half-divergence angle of lens with focal length of 15 cm is around 0.7°. Performing the calculation of electric field intensity maxima for different incidence

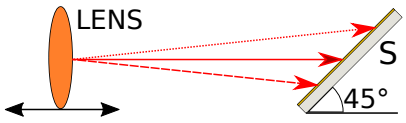

Fig. 8. Schematic layout of beam alignment. Lens position influence on beam position on sample (S).

angles around 45°, we estimate the maximum difference in EFI maxima to be 1.4%. Thus, we can not explain the observed differences in LIDT fluences using the beam divergence determined by the Gaussian beam approximation. However, the difference in EFI maxima could be added into the error bars when the sample plane was far from focus.

F. Alignment

During the LIDT test we changed the positions of focusing lens along the beam axis. As the lens was moving step by step from one extreme position to the second one, there was a gradual movement of the beam peak in the plane perpendicular to the beam propagation. This movement occurred in both horizontal and vertical coordinates and was recorded by a beam profiling camera. Since the LIDT tests were done at 45° incidence angle, see Fig. 8, the change of peak position in horizontal plane can be projected also along the beam axis and thus influence the lens-sample distance.

Assuming approximately the same distance changes along the beam axis as in horizontal coordinates ($\Delta x \approx \Delta z$), we can estimate the error in LIDT fluence by expressing the ratio between effective areas located at lens positions of Δz difference. We estimate the effective area (A_{eff}) difference as:

$$\frac{\Delta A_{\text{eff}}}{A_{\text{eff}}}(z_i) = \frac{\max\left[A_{\text{eff}}(z_i + \frac{\Delta z_i}{2}), A_{\text{eff}}(z_i - \frac{\Delta z_i}{2})\right]}{\min\left[A_{\text{eff}}(z_i + \frac{\Delta z_i}{2}), A_{\text{eff}}(z_i - \frac{\Delta z_i}{2})\right]}, \tag{9}$$

where z_i means i-th lens position. For the large range of lens positions associated with horizontal movement of beam $\sim$ 400 µm, i.e. $\bigtriangledown$ and $\square$ datasets on Fig. 6a) and 6b), respectively, the beam positioning error could be $\sim$ 5 %. In the case of $\bigtriangleup$ and $\diamond$ datasets, the error caused by 30 µm peak position movement can be neglected ($<$ 0.5 %). The data of pointing stability show standard deviation lower than 10 µm and thus the parameter can be ignored.

The move of peak position indicates that there could be also some influence on incidence angle (and EFI maximum) when the lens is moved. We can estimate the incidence angle change as:

$$\Delta\theta \sim \arctan\left(\frac{\Delta x}{f_{15}}\right). \tag{10}$$

In the case of $\Delta x = 400$ µm, the $\Delta\theta \sim 0.15°$ corresponds to difference in EFI maxima $\leq$ 0.3 %. Thus, the influence of beam positioning on EFI maxima does not play an important role. However, the effective area differences due to beam displacement calculated using Eq. 9 could be used for explanation of the differences between the LIDT test campaigns presented on Fig. 6.

G. Camera errors

G.1. Noise error

The BP87 camera shows very low noise level around 0.1 % of signal maximum. Furthermore, several beam profile measurements with different background area selection confirmed the

same LIDT results. Thus, we do not consider the noise error as important.

G.2. Pixel size error

The effective area determination is limited by the spatial resolution of the beam profiler given by the pixel size. [51] In the tests with lens of 15 cm focal length, the pixel size $l_{\text{pixel}} = 3.45\,\mu\text{m}$. Taking into account an absolute error of effective beam diameter determination, i.e. $\delta d_{\text{eff}} = \pm l_{\text{pixel}}$, we assess the relative error:[51]

$$\epsilon_{\text{pixel}} = \frac{\delta A_{\text{eff}}}{A_{\text{eff}}} = \frac{\frac{\pi}{2} d_{\text{eff}} \delta d_{\text{eff}}}{\pi \frac{d_{\text{eff}}^2}{4}} = \pm \frac{2 \cdot l_{\text{pixel}}}{d_{\text{eff}}}. \quad (11)$$

The problem of spatial resolution is a serious issue when beam profilers are used to measure relatively small spots. For our lens with 15 cm focal length, the minimum effective beam diameter $d_{\text{eff}} \approx 40\,\mu\text{m}$ corresponds to the relative error $\epsilon_{\text{pixel}} \approx 17\,\%$. This error could be one of the main reasons why the LIDT results on Figs. 6a) and 6b) show such high dispersion for smaller beam sizes.

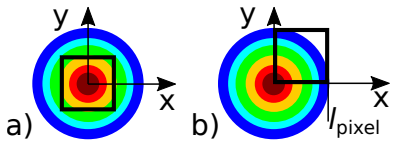

Fig. 9. Schematic drawing of Gaussian beam intensity peak: a) at the center of pixel, b) at the corner of pixel.

G.3. Maximum pixel intensity error

We will estimate an error of maximum intensity value measured on one pixel of our camera by considering difference between two extreme cases of maximum pixel positioning, i.e. the case of peak at the center of pixel (Fig. 9a) and the case when maximum intensity is at the corner of pixel (Fig. 9b). Assuming Gaussian intensity profile, we can determine h, the mean value of intensity within the S_{pixel} pixel area by:

$$h = \iint_{S_{\text{pixel}}} \exp\left(\frac{-4\left(x^2+y^2\right)}{d_{\text{eff}}^2}\right) dx\,dy / S_{\text{pixel}}, \quad (12)$$

where d_{eff} is the effective beam diameter and x, y are transverse coordinates. Integrating the Eq. 12 from $-l_{\text{pixel}}/2$ to $l_{\text{pixel}}/2$ over both x, y coordinates, we defined the h value in the case of intensity peak at the center of pixel, see Fig. 9a). For the intensity peak at the corner of pixel, the integral was from 0 to l_{pixel} in both x, y coordinates. Using the $l_{\text{pixel}} = 3.45\,\mu\text{m}$, the maximal difference between h values is $\epsilon_{\text{max pixel}} \approx 1.5\,\%$. In the case of intensity peak at pixel corner, the h value is by 2 % lower than intensity peak of Gaussian beam with $d_{\text{eff}} = 40\,\mu\text{m}$.

G.4. Camera contrast error

The error resulting from the discrete irradiance levels can be assessed as: [51]

$$\epsilon_{\text{contrast}} = 1/\tilde{V}_{xy}, \quad (13)$$

where $\tilde{V}_{xy}$ represents the average value of V_{xy} voltages inside the software aperture, expressed in digitized grey levels that are proportional to the light energy collected by each pixel of the array. We found $\epsilon_{\text{contrast}} \approx 0.03\,\%$.

G.5. Camera linearity error

The non-linearity error is expressed as: [51]

$$\epsilon_{\text{lin}} = 10^{-2} \cdot \tilde{V}_{xy}/2^{(DR)}, \quad (14)$$

where $2^{(DR)}$ means the dynamic range of camera represented by the number of grey levels. We found $\epsilon_{\text{lin}} \approx 0.01\,\%$. Thus, the camera linearity and contrast errors are negligible.

H. Other errors

Other errors in measurement might include the accuracy of motorized stage movements or the accuracy of microscopic observation. The latter mentioned we estimate to be around low percentage units.

Table 4. Synthesis of error margins for identified contributors in the best case scenario of LIDT tests with lens of 30 cm focal length. A_{eff} - effective beam area, AOI - angle of incidence, EFI - electric field intensity. With quadratic summation, an accuracy of 9% can be achieved for the determination of LIDT fluences. The pulse energies and A_{eff} matching error corresponds to shift in lens position by 0.1 mm.

No.	Contributor	Error bar
1	Beam size variations (3σ)	6%
2	Damage detection	5%
3	Beam positioning at 45° AOI	3%
4	Calorimeter	3%
5	Pulse energies and A_{eff} matching	2%
6	Pulse energy variations (3σ)	0.7%
7	Pulse energy increment	0.5%
8	Effect of beam divergence	0.5%
9	Effect of AOI on EFI maximum	0.3%
	Total budget	21%
	Quadratic summation	9%

4. CONCLUSION

In our particular case, the LIDT results, obtained by lens with 30 cm focal length in the range of effective beam diameters between 80 and 160 µm, show that the sub-picosecond damage threshold of dielectric coatings is independent of beam size as shown on Fig. 5b). In order to evaluate the tests of such optical components as accurately as possible, we provide in Table 4 a synthesis of identified contributors to errors. As the major error contributor in the best case scenario, we detected the 3σ variations of beam size (6%). The influence of contributors related to beam alignment, i.e. beam positioning at 45° incidence angle, pulse energies and effective areas matching, beam divergence or effect of incidence angle on EFI maximum, could be minimized by damage testing at normal incidence or by beam profile measurement at the same incidence angle as the tests are performed.

In contrast to the results with lens of 30 cm focal length, it is difficult to determine the relation between beam size and LIDT fluence in the case of lens with smaller focal length of 15 cm.

The different fluences before and after the beam waist (Fig. 7) could suggest potential beam deformation related with self-focusing in the lens. Another error could rise from beam profile measurements, especially for smaller beam sizes. This could be related to pixel size error of 17 % or maximum pixel intensity error of 1.5 %. Last but not least, it is necessary to emphasize the significant effect of the chosen shift in lens positions to the intrinsic LIDT fluence in respect to the effective beam diameters, see Fig. 4.

From the practical point of view, this study recommends in our case the lens of 30 cm focal length to be used for LIDT testing of optical components intended e.g. for use in larger beam laser systems. The lens of 15 cm focal length, by contrast, should not be used for damage testing since the uncertainties in LIDT fluence, regardless of their nature, are too large.

On the more general perspective, this work underlines the difficulty of LIDT measurements with very focused laser beams. Despite our best efforts, the deviations of LIDT are quite large and we believe similar issues should have been encountered in previous studies related to this topic, see Table 1, where spot size dependences were observed for highly focused beams.

Funding. This project has received funding from the European Union's Horizon 2020 research and innovation programme under the Marie Skłodowska-Curie grant agreement No. 813159.

Acknowledgements. We thank L. Lamaignère for fruitful discussions and ideas about the work.

Disclosures. The authors declare no conflicts of interest.

Data availability. Data underlying the results presented in this paper are not publicly available at this time but may be obtained from the authors upon reasonable request.

REFERENCES

1. M. Soileau, "Laser-Induced Damage Phenomena in Optics: A Historical Overview," in *Laser-Induced Damage in Optical Materials,* D. Ristau, ed. (CRC Press, 2014), pp. 3–8.
2. W. Koechner, "Damage of Optical Elements," in *Solid-State Laser Engineering,* vol. 1 (Springer New York, New York, NY, 2006), pp. 680–701. Series Title: Springer Series in Optical Sciences.
3. D. Bäuerle, "Introduction," in *Laser Processing and Chemistry,* (Springer Berlin Heidelberg, Berlin, Heidelberg, 2011), pp. 3–12.
4. R. R. Gattass and E. Mazur, "Femtosecond laser micromachining in transparent materials," Nat. Photonics **2**, 219–225 (2008).
5. N. Bloembergen, "Role of Cracks, Pores, and Absorbing Inclusions on Laser Induced Damage Threshold at Surfaces of Transparent Dielectrics," Appl. Opt. **12**, 661 (1973).
6. L. G. DeShazer, B. E. Newnam, and K. M. Leung, "Role of coating defects in laser-induced damage to dielectric thin films," Appl. Phys. Lett. **23**, 607–609 (1973).
7. N. L. Boling and G. Dubé, "Laser-induced inclusion damage at surfaces of transparent dielectrics," Appl. Phys. Lett. **23**, 658–660 (1973).
8. R. H. Picard, D. Milam, and R. A. Bradbury, "Statistical analysis of defect-caused laser damage in thin films," Appl. Opt. **16**, 1563 (1977).
9. J. Reif, S. Petzoldt, A. P. Elg, and E. Matthias, "The role of defects in laser surface damage thresholds of fluoride crystals," Appl. Phys. A Solids Surfaces **49**, 199–204 (1989).
10. F. E. Hovis, B. A. Shepherd, C. T. Radcliffe, A. L. Bailey, and W. T. Boswell, "Optical damage at the part per million level: the role of trace contamination in laser-induced optical damage," (Boulder, CO, 1994), p. 145.
11. J.-Y. Natoli, L. Gallais, H. Akhouayri, and C. Amra, "Laser-induced damage of materials in bulk, thin-film, and liquid forms," Appl. Opt. **41**, 3156 (2002).
12. G. Duchateau, M. D. Feit, and S. G. Demos, "Strong nonlinear growth of energy coupling during laser irradiation of transparent dielectrics and its significance for laser induced damage," J. Appl. Phys. **111**, 093106 (2012).
13. Y. Xu, D. H. Dunlap, L. A. Emmert, and W. Rudolph, "Laser-driven detonation wave in hafnium oxide film: Defect controlled laser damage and ablation," J. Appl. Phys. **128**, 123101 (2020).
14. B. C. Stuart, M. D. Feit, S. Herman, A. M. Rubenchik, B. W. Shore, and M. D. Perry, "Nanosecond-to-femtosecond laser-induced breakdown in dielectrics," Phys. Rev. B **53**, 1749–1761 (1996).
15. D. Du, X. Liu, G. Korn, J. Squier, and G. Mourou, "Laser-induced breakdown by impact ionization in sio$_2$ with pulse widths from 7 ns to 150 fs," Appl. Phys. Lett. **64**, 3071–3073 (1994).
16. A. Joglekar, H. Liu, G. Spooner, E. Meyhöfer, G. Mourou, and A. Hunt, "A study of the deterministic character of optical damage by femtosecond laser pulses and applications to nanomachining," Appl. Phys. B **77**, 25–30 (2003).
17. B. Mangote, L. Gallais, M. Zerrad, F. Lemarchand, L. H. Gao, M. Commandré, and M. Lequime, "A high accuracy femto-/picosecond laser damage test facility dedicated to the study of optical thin films," Rev. Sci. Instruments **83**, 013109 (2012).
18. M. Garcia-Lechuga, G. Gebrayel El Reaidy, H. Ning, P. Delaporte, and D. Grojo, "Assessing the limits of determinism and precision in ultrafast laser ablation," Appl. Phys. Lett. **117**, 171604 (2020).
19. B. Zhou, A. Kar, M. J. Soileau, and X. Yu, "Invariance of the r ^{2} - ln(F) relationship and attainable precision in ultrafast laser ablation experiments," Opt. Express **29**, 5635 (2021).
20. B. C. Stuart, M. D. Feit, S. Herman, A. M. Rubenchik, B. W. Shore, and M. D. Perry, "Optical ablation by high-power short-pulse lasers," J. Opt. Soc. Am. B **13**, 459–468 (1996).
21. A. Rosenfeld, M. Lorenz, R. Stoian, and D. Ashkenasi, "Ultrashort-laser-pulse damage threshold of transparent materials and the role of incubation," Appl. Phys. A: Mater. Sci. & Process. **69**, S373–S376 (1999).
22. N. Sanner, B. Bussiere, O. Utéza, A. Leray, T. Itina, M. Sentis, J. Y. Natoli, and M. Commandré, "Influence of the beam-focus size on femtosecond laser-induced damage threshold in fused silica," in *Commercial and Biomedical Applications of Ultrafast Lasers VIII,* vol. 6881 J. Neev, S. Nolte, A. Heisterkamp, and C. B. Schaffer, eds. (San Jose, CA, 2008), p. 68810W.
23. O. Uteza, B. Bussiere, F. Canova, J.-P. Chambaret, P. Delaporte, T. Itina, and D. Zeitoun, "Laser-induced damage threshold of sapphire in nanosecond, picosecond and femtosecond regimes," Appl. Surf. Sci. **254**, 799–803 (2007).
24. T. A. Laurence, R. A. Negres, S. Ly, N. Shen, C. W. Carr, D. A. Alessi, A. Rigatti, and J. D. Bude, "Role of defects in laser-induced modifications of silica coatings and fused silica using picosecond pulses at 1053 nm: Ii. scaling laws and the density of precursors," Opt. Express **25**, 15381–15401 (2017).
25. S. Martin, A. Hertwig, M. Lenzner, J. Krüger, and W. Kautek, "Spot-size dependence of the ablation threshold in dielectrics for femtosecond laser pulses," Appl. Phys. A: Mater. Sci. & Process. **77**, 883–884 (2003).
26. A. Hertwig, S. Martin, J. Krüger, and W. Kautek, "Interaction area dependence of the ablation threshold of ion-doped glass," Thin Solid Films **453-454**, 527–530 (2004).
27. D. Ashkenasi and A. Rosenfeld, "Material processing of dielectrics with femtosecond lasers," in *Laser Applications in Microelectronic and Optoelectronic Manufacturing IV,* vol. 3618 J. J. Dubowski, H. Helvajian, E.-W. Kreutz, and K. Sugioka, eds., International Society for Optics and Photonics (SPIE, 1999), pp. 102 – 113.
28. O. Armbruster, A. Naghilou, M. Kitzler, and W. Kautek, "Spot size and pulse number dependence of femtosecond laser ablation thresholds of silicon and stainless steel," Appl. Surf. Sci. **396**, 1736–1740 (2017).
29. A. Naghilou, O. Armbruster, and W. Kautek, "Femto- and nanosecond pulse laser ablation dependence on irradiation area: The role of defects in metals and semiconductors," Appl. Surf. Sci. **418**, 487–490 (2017).
30. B.-M. Kim, M. D. Feit, A. M. Rubenchik, E. J. Joslin, J. Eichler, P. C. Stoller, and L. B. Da Silva, "Effects of high repetition rate and beam

size on hard tissue damage due to subpicosecond laser pulses," Appl. Phys. Lett. **76**, 4001–4003 (2000).
31. A. Naghilou, O. Armbruster, M. Kitzler, and W. Kautek, "Merging Spot Size and Pulse Number Dependence of Femtosecond Laser Ablation Thresholds: Modeling and Demonstration with High Impact Polystyrene," The J. Phys. Chem. C **119**, 22992–22998 (2015).
32. O. Armbruster, A. Naghilou, and W. Kautek, "The Role of Defects in Pulsed Laser Matter Interaction," in *Advances in the Application of Lasers in Materials Science,* vol. 274 P. M. Ossi, ed. (Springer International Publishing, Cham, 2018), pp. 39–61. Series Title: Springer Series in Materials Science; Excellent LID introduction.
33. J. B. Ashcom, R. R. Gattass, C. B. Schaffer, and E. Mazur, "Numerical aperture dependence of damage and supercontinuum generation from femtosecond laser pulses in bulk fused silica," J. Opt. Soc. Am. B **23**, 2317–2322 (2006).
34. S. R. Foltyn, "Spotsize effects in laser damage testing," Laser Induc. Damage Opt. Mater. pp. 368–379 (1982).
35. L. Lamaignère, M. Balas, R. Courchinoux, T. Donval, J. C. Poncetta, S. Reyné, B. Bertussi, and H. Bercegol, "Parametric study of laser-induced surface damage density measurements: Toward reproducibility," J. Appl. Phys. **107**, 023105 (2010).
36. L. Gallais, X. Cheng, and Z. Wang, "Influence of nodular defects on the laser damage resistance of optical coatings in the femtosecond regime," Opt. Lett. **39**, 1545–1548 (2014).
37. M. Sozet, J. Néauport, E. Lavastre, N. Roquin, L. Gallais, and L. Lamaignère, "Laser damage density measurement of optical components in the sub-picosecond regime," Opt. Lett. **40**, 2091 (2015).
38. L. Lamaignère, A. Ollé, M. Chorel, N. Roquin, A. A. Kozlov, B. N. Hoffman, J. B. Oliver, S. G. Demos, L. Gallais, R. A. Negres, and A. Melninkaitis, "Round-robin measurements of the laser-induced damage threshold with sub-picosecond pulses on optical single layers," Opt. Eng. **60** (2020).
39. M. Scherer, "Magnetron sputter-deposition on atom layer scale," Vakuum Forschung und Praxis **21**, 24–30 (2009).
40. ISO 21254-1:2011, "Lasers and laser-related equipment – test methods for laser-induced damage threshold – part 1: Definitions and general principles," Tech. rep., International Organization for Standardization, Geneva, Switzerland (2011).
41. A. Ollé, J. Luce, N. Roquin, C. Rouyer, M. Sozet, L. Gallais, and L. Lamaignère, "Implications of laser beam metrology on laser damage temporal scaling law for dielectric materials in the picosecond regime," Rev. Sci. Instruments **90**, 073001 (2019).
42. L. Emmert and W. Rudolph, "Femtosecond Laser-Induced Damage in Dielectric Materials," in *Laser-Induced Damage in Optical Materials,* D. Ristau, ed. (CRC Press, 2014), pp. 127–152.
43. K. Ohta and H. Ishida, "Matrix formalism for calculation of electric field intensity of light in stratified multilayered films," Appl. Opt. **29**, 1952 (1990).
44. A. V. Smith and B. T. Do, "Bulk and surface laser damage of silica by picosecond and nanosecond pulses at 1064 nm," Appl. Opt. **47**, 4812 (2008).
45. E. T. J. Nibbering, G. Grillon, M. A. Franco, B. S. Prade, and A. Mysyrowicz, "Determination of the inertial contribution to the nonlinear refractive index of air, N_2, and O_2 by use of unfocused high-intensity femtosecond laser pulses," J. Opt. Soc. Am. B **14**, 650 (1997).
46. Y. E. Geints, A. M. Kabanov, A. A. Zemlyanov, E. E. Bykova, O. A. Bukin, and S. S. Golik, "Kerr-driven nonlinear refractive index of air at 800 and 400 nm measured through femtosecond laser pulse filamentation," Appl. Phys. Lett. **99**, 181114 (2011).
47. A. Börzsönyi, Z. Heiner, A. Kovács, M. P. Kalashnikov, and K. Osvay, "Measurement of pressure dependent nonlinear refractive index of inert gases," Opt. Express **18**, 25847 (2010).
48. V. Loriot, E. Hertz, O. Faucher, and B. Lavorel, "Measurement of high order Kerr refractive index of major air components: erratum," Opt. Express **18**, 3011 (2010).
49. J. Schwarz, P. Rambo, M. Kimmel, and B. Atherton, "Measurement of nonlinear refractive index and ionization rates in air using a wavefront sensor," Opt. Express **20**, 8791 (2012).
50. A. V. Mitrofanov, A. A. Voronin, D. A. Sidorov-Biryukov, G. Andriukaitis, T. Flöry, A. Pugžlys, A. B. Fedotov, J. M. Mikhailova, V. Y. Panchenko, A. Baltuška, and A. M. Zheltikov, "Post-filament self-trapping of ultrashort laser pulses," Opt. Lett. **39**, 4659 (2014).
51. Aurel Stratan, Alexandru Zorila, Laurentiu Rusen, and George Nemes, "Measuring effective area of spots from pulsed laser beams," Opt. Eng. **53**, 1–11 (2014).